Comparison and evaluation of Hall thruster models

G. J. M. Hagelaar, J. Bareilles, L. Garrigues, and J.-P. Boeuf
CPAT, Bâtiment 3R2, Université Paul Sabatier
118 Route de Narbonne, Toulouse, France
hagelaar@cpat.ups-tlse.fr

Principal Investigator: JP Boeuf, Tel +33 61 55 68 60, e-mail jpb@cpat.ups-tlse.fr

Final report – 20 March 2002 – EOARD contract N° F61775-01-WE015

The Contractor, ADPA, University Paul Sabatier, hereby declares that, to the best of its knowledge and belief, the technical data delivered herewidth under Contract N° F61775-01-WE015 is complete, accurate, and complies with all requirements of the contracts.

DATE: 27/03/2002
Name and Title of Authorized Official: J. BONNET, President

I certify that there were no subject inventions to declare as defined in FAR 52.227-13 during the performance of this contract.

DATE: 27/03/2002
Name and Title of Authorized Official: J. BONNET, President

REPORT DOCUMENTATION PAGE

Form Approved OMB No. 0704-0188

1. REPORT DATE (DD-MM-YYYY)	2. REPORT TYPE	3. DATES COVERED (FROM - TO)
04-04-2002	Final rept.	20-04-2001 to 20-04-2002

4. TITLE AND SUBTITLE
comparisons and Evaluation of Hall Thruster Models
Unclassified

5a. CONTRACT NUMBER
F61775-01-WF015

5b. GRANT NUMBER

5c. PROGRAM ELEMENT NUMBER

6. AUTHOR(S)
Hagelaar, G. L. ;
Bareilles, J. ;
Garrigues, L. ;
Boeuf, J-P ;

5d. PROJECT NUMBER

5e. TASK NUMBER

5f. WORK UNIT NUMBER

7. PERFORMING ORGANIZATION NAME AND ADDRESS
Universite Paul Sabatier
118 Route de Narbonne
Toulouse 31062, Francexxxxx

8. PERFORMING ORGANIZATION REPORT NUMBER

9. SPONSORING/MONITORING AGENCY NAME AND ADDRESS
EOARD
PSC 802 Box 14
FPO, xx09499-0014

10. SPONSOR/MONITOR'S ACRONYM(S)

11. SPONSOR/MONITOR'S REPORT NUMBER(S)

12. DISTRIBUTION/AVAILABILITY STATEMENT
APUBLIC RELEASE
,

13. SUPPLEMENTARY NOTES

14. ABSTRACT

The aim of the project is to compare, evaluate, and possibly improve the following two SPT models: 1) The two-dimensional hybrid model developed at the MIT between 1994 and 1998, by Mike Fife and Manuel Martinez-Sanchez. 2) The two-dimensional hybrid model developed at the CPAT from 2000 to present, by the authors of this report. Both models attempt to provide a complete simulation of the temporal and spatial behavior of the SPT discharge, combining a particle description of neutrals and ions with a fluid description of electrons, where the electric field is obtained from assuming quasi-neutrality. In the first and main part of this report we break the models down into components, which we describe, compare, and discuss in detail. In the second part of the report we check for gross numerical errors in the models, by slightly modifying them so as to represent similar physics, and then comparing their results.

15. SUBJECT TERMS
EOARD; Modelling & Simulation; Hall effect thrusters

16. SECURITY CLASSIFICATION OF:			17. LIMITATION OF ABSTRACT	18. NUMBER OF PAGES	19. NAME OF RESPONSIBLE PERSON
a. REPORT	b. ABSTRACT	c. THIS PAGE	Public Release	19	Fenster, Lynn lfenster@dtic.mil
Unclassified	Unclassified	Unclassified			19b. TELEPHONE NUMBER International Area Code Area Code Telephone Number 703767-9007 DSN 427-9007

REPORT DOCUMENTATION PAGE

Form Approved OMB No. 0704-0188

1. REPORT DATE *(DD-MM-YYYY)*	2. REPORT TYPE	3. DATES COVERED *(From – To)*
04-04-2002	Final Report	20 April 2001 - 20-Apr-02

4. TITLE AND SUBTITLE

Comparisons and Evaluation of Hall Thruster Models

5a. CONTRACT NUMBER
F61775-01-WE015

5b. GRANT NUMBER

5c. PROGRAM ELEMENT NUMBER

6. AUTHOR(S)

GLM Hagelaar, J Bareilles, L Garrigues, and J-P Boeuf

5d. PROJECT NUMBER

5d. TASK NUMBER

5e. WORK UNIT NUMBER

7. PERFORMING ORGANIZATION NAME(S) AND ADDRESS(ES)

Universite Paul Sabatier
118 Route de Narbonne
Toulouse 31062
France

8. PERFORMING ORGANIZATION REPORT NUMBER

N/A

9. SPONSORING/MONITORING AGENCY NAME(S) AND ADDRESS(ES)

European Office of Aerospace Research and Development
PSC 802 BOX 14
FPO 09499-0014

10. SPONSOR/MONITOR'S ACRONYM(S)
EOARD/AFOSR

11. SPONSOR/MONITOR'S REPORT NUMBER(S)
SPC 01-4015

12. DISTRIBUTION/AVAILABILITY STATEMENT

Approved for public release; distribution is unlimited.

13. SUPPLEMENTARY NOTES

14. ABSTRACT

The aim of the project is to compare, evaluate, and possibly improve the following two SPT models:

1) The two-dimensional hybrid model developed at the MIT between 1994 and 1998, by Mike Fife and Manuel Martinez-Sanchez.
2) The two-dimensional hybrid model developed at the CPAT from 2000 to present, by the authors of this report.

Both models attempt to provide a complete simulation of the temporal and spatial behavior of the SPT discharge, combining a particle description of neutrals and ions with a fluid description of electrons, where the electric field is obtained from assuming quasi-neutrality. In the first and main part of this report we break the models down into components, which we describe, compare, and discuss in detail. In the second part of the report we check for gross numerical errors in the models, by slightly modifying them so as to represent similar physics, and then comparing their results.

15. SUBJECT TERMS
EOARD, Modelling & Simulation, Hall effect thrusters

16. SECURITY CLASSIFICATION OF:			17. LIMITATION OF ABSTRACT	18, NUMBER OF PAGES	19a. NAME OF RESPONSIBLE PERSON
a. REPORT	b. ABSTRACT	c. THIS PAGE			Ingrid Wysong
UNCLAS	UNCLAS	UNCLAS	UL	18	19b. TELEPHONE NUMBER *(Include area code)* +44 (0)20 7514 4285

Comparison and evaluation of Hall thruster models

G. J. M. Hagelaar, J. Bareilles, L. Garrigues, and J.-P. Boeuf
CPAT, Bâtiment 3R2, Université Paul Sabatier
118 Route de Narbonne, Toulouse, France
hagelaar@cpat.ups-tlse.fr

Final report – 20 March 2002 – EOARD contract N° F61775-01-WE015

1 INTRODUCTION

This is the final report on the research project conducted at the CPAT for the US Airforce, on Hall thrusters, called stationary plasma thrusters (SPTs) in the following. The aim of the project is to compare, evaluate, and possibly improve the following two SPT models:

1) The two-dimensional hybrid model developed at the MIT between 1994 and 1998, by Mike Fife and Manuel Martinez-Sanchez, and documented in [Fif98].
2) The two-dimensional hybrid model developed at the CPAT from 2000 to present, by the authors of this report, and documented in [Hag01] and [Hag02].

Both models attempt to provide a complete simulation of the temporal and spatial behavior of the SPT discharge, combining a particle description of neutrals and ions with a fluid description of electrons, where the electric field is obtained from assuming quasi-neutrality.
In the first and main part of this report we break the models down into components, which we describe, compare, and discuss in detail. We consider the following topics:

In the second part of the report we check for gross numerical errors in the models, by slightly modifing them so as to represent similar physics, and then comparing their results.

2 DESCRIPTION AND COMPARISON OF MODEL COMPONENTS

2.1 Geometry and grid

The MIT and CPAT models represent only the axial and radial dimensions of the SPT geometry and discharge; azimuthal symmetry is assumed. The computational domain, which comprises both the discharge channel and the near exterior of the thruster, is schematically shown in figure 1; the full discharge simulation is carried out only within a certain region that is confined by physical walls and magnetic field lines.
The two models use different computational grids; see figure 2. The MIT model has a non-uniform conformal grid that may be adapted to arbitrarily shaped channel walls. The rectangular grid of the CPAT model does not offer this possibility, but on the other hand leads to much simpler, and thus faster, computation. Inside the channel both grids are about equally refined; typically a grid cell measures 1 mm ×1 mm.

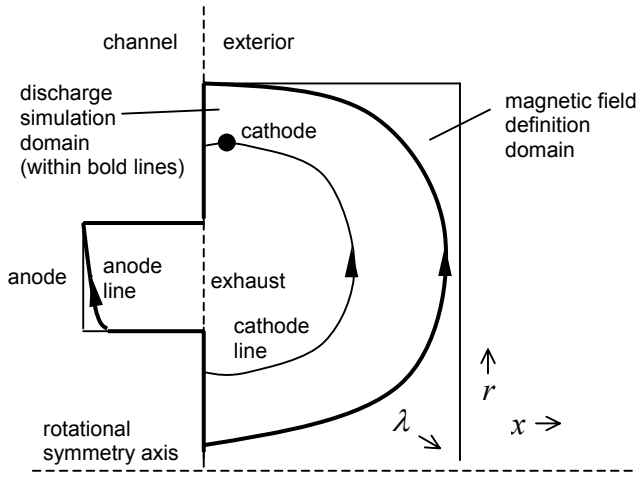

Figure 1. Schematic picture of the computational domain.

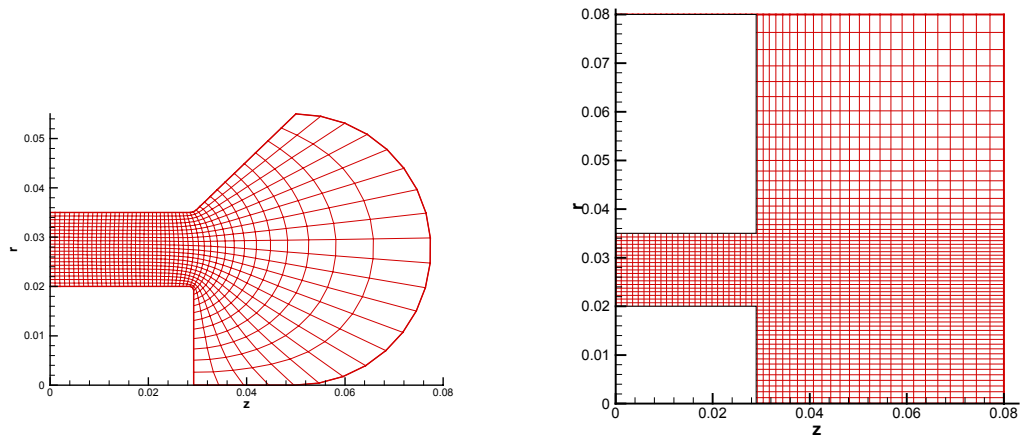

Figure 2. Comparison between the computational grids of MIT model on the left-hand side and the CPAT model on the right.

2.2 Magnetic field and stream function

The magnetic field is assumed to be entirely determined by the electromagnets and to be unaffected by the discharge, so that it can be treated as input data. Both models calculate, to facilitate the solution of the electron transport equations, a magnetic stream function λ from

$$\frac{\partial \lambda}{\partial x} = rB_r \text{ and } \frac{\partial \lambda}{\partial r} = -rB_x , \quad (1)$$

where x and r are the axial and radial position coordinates and B_x and B_r are the axial and radial components of the magnetic field. The λ defined by these equations is constant along magnetic field lines ($\mathbf{B}\cdot\nabla\lambda = 0$) and usually increases monotonically from anode to cathode. The cross field gradient of any quantity Q can be expressed in terms of λ as

$$\nabla_{\perp} Q = rB\frac{\partial Q}{\partial \lambda} . \quad (2)$$

An additional computational grid is attached to the λ-coordinate with intervals that have approximately the same size as the cells of the x-r-grid.

2.3 Neutral atoms

In both models the density of neutral xenon atoms in the thruster, essential to find the ionization rate and the electrical conductivity of the plasma, is obtained from a Monte Carlo simulation. That is, the individual paths of a large number of neutrals are calculated, where collisions are treated with random numbers. This approach is realistic but takes much computation time and introduces statistical errors. The neutrals are introduced in the simulation at a certain injection region at the anode and are followed until they reach the right boundary of the geometry. Additional neutrals are introduced at the channel walls to account for wall-recombination of ions. The initial neutral velocity distribution is randomly sampled from a half-Maxwellian distribution; see section 2.4. Only collisions with walls are considered, in which the neutrals are isotropically scattered.

In both models neutral loss by ionization is implemented by the following procedure: To each simulated neutral a certain weight w is attributed, which gradually decreases in time as

$$w = w_0 \exp(-nk_i t), \quad (3)$$

where w_0 is the initial weight, n is the local plasma density, k_i is the ionization rate coefficient dependent on the local electron mean energy, and t is the time. This technique leads to better statistics than simply eliminating neutrals from the simulation according to their ionization probability, especially beyond the exhaust where the neutral density may be quite low.

2.4 Sampling of neutral atoms

Confusion may easily come about on how to properly determine random initial velocities for the neutral atoms in the Monte-Carlo model. The MIT and CPAT models use different but in fact equivalent methods. Here we document these methods.

The neutrals are introduced at the anode per unit time and per unit surface; they are thus sampled from the neutral flux crossing the anode plane, i.e. from the neutral flux in the axial direction. For a Maxwellian velocity distribution the axial flux in the Cartesian velocity interval $\mathrm{d}v_x\mathrm{d}v_y\mathrm{d}v_y$ around (v_x, v_y, v_z) is

$$g(v_x,v_y,v_z)\,\mathrm{d}v_x\mathrm{d}v_y\mathrm{d}v_z \propto v_x \exp\left(-\frac{Mv_x^2}{2kT}\right)\exp\left(-\frac{Mv_y^2}{2kT}\right)\exp\left(-\frac{Mv_z^2}{2kT}\right)\mathrm{d}v_x\mathrm{d}v_y\mathrm{d}v_z , \quad (4)$$

where k is the Boltzmann constant, T is the atom temperature, and M the atom mass.

The MIT models samples directly from this distribution as

$$v_x = \sqrt{\frac{kT}{2m}\ln(R_1)} \tag{5}$$

$$v_y = \sqrt{\frac{kT}{2m}\ln(R_2)}\cos(2\pi R_3) \tag{6}$$

$$v_z = \sqrt{\frac{kT}{2m}\ln(R_2)}\sin(2\pi R_3) \tag{7}$$

where $R_{1\text{-}3}$ are random numbers on [0,1]; see also the book of Bird [Bir94]. On average v_x is larger than v_y and v_z because we sample from an axial flux, not from a density.
In an alternative approach the CPAT model uses the distribution in spherical coordinates

$$g(v,\cos\theta,\phi)\, v^2 \sin\theta \; \mathrm{d}v\mathrm{d}\theta\mathrm{d}\phi \propto v^3 \exp\left(-\frac{mv^2}{2kT}\right)\sin\theta\cos\theta \; \mathrm{d}v\mathrm{d}\theta\mathrm{d}\phi \tag{8}$$

where v is the speed, θ the angle with the axial direction, and ϕ an angle in the plane perpendicular to the axis. Random values for these coordinates now follow from

$$\left(1+\frac{mv^2}{2kT}\right)\exp\left(-\frac{mv^2}{2kT}\right) = R_1 \tag{9}$$

$$\cos\theta = \sqrt{R_2} \tag{10}$$

$$\phi = 2\pi R_3 \tag{11}$$

where $R_{1\text{-}3}$ are once again three random numbers. The problem here is that the equation for the speed v has no analytical solution and requires a few Newton iterations. On the other hand, the equations for θ and ϕ are extremely useful since they apply not only to a Maxwellian distribution, but to any isotropic distribution; for instance, they can be used together with a fixed value for the speed to simulate mono-energetic particles.
Analogous formulas are being used for neutrals scattered isotropically at the walls or coming off the walls from recombination. Note that in this case the radial direction takes the role played in the above formulas by the axial direction.
Typically the MIT model uses a higher initial neutral temperature than the CPAT model: 1000 K, against 500 K for the CPAT model. The MIT value is based on measurements of the anode temperature.

2.5 Accommodation to the wall temperature

The MIT model assumes that the neutrals accommodate to the wall temperature when colliding with the channel walls. The neutral temperature after a wall collision is calculated as

$$\frac{3}{2}kT_a = \alpha\frac{3}{2}kT_w + (1-\alpha)\frac{1}{2}Mv^2 \tag{12}$$

where α is the accommodation coefficient, T_w is the wall temperature, and $Mv^2/2$ is the energy of the incident neutral; typically α = 0.8 and T_w = 900 K constant along the channel. The neutral velocity after the collision is draw randomly from a half-Maxwellian distribution at temperature T_a.
The CPAT model does not include wall accommodation. Wall collisions only change the direction of the neutral velocity, not its magnitude. A random direction is found from equations (10) and (11).
Note that even for α = 0 the MIT model differs from the CPAT model. We remark that the wall-accommodation procedure of the MIT model is odd: it involves treating a single particle's energy as if it were a mean energy, which might lead to undesirable artifacts. It would be better to treat the accommodation as follows: First find a random speed v_w from a half-Maxwellian distribution at the wall temperature; this can be done either directly from equation (9) or indirectly from three components (5)-(7). Subsequently the accommodated neutral speed after the wall collision can be taken as

$$v_a = \sqrt{\alpha v_w^{\,2} + (1-\alpha)v^2}\,, \tag{13}$$

with v the incident speed, and the direction can be found from equations (10) and (11), as in the CPAT model.

2.6 Ions

Like the neutrals, the ions are in both models described by a Monte Carlo simulation. They are introduced in the simulation at positions that are randomly chosen according to the ionization rate profile. The initial ion velocity distribution is isotropic and Maxwellian at the neutral gas temperature. The ions are assumed to be accelerated by the electric field only, i.e. to be insensitive to the magnetic field. They are followed until they reach any of the boundaries of the simulation domain; ions striking the walls are thus assumed to recombine at the surface. Besides the ion density, the ion Monte Carlo simulation yields the ion flux and the ion energy distribution.
The MIT model distinguishes between singly and doubly charge ions, whereas the CPAT model assumes all ions to be singly charged. Although the doubly charged ions in the MIT model may make up for about 10% of the total ion flux, the double ionization seems to have little influence on the discharge in the channel.

2.7 Basic electron equations

The models describe the electrons by a set of fluid equations, which we document in this section. We use the formalism of the CPAT model; although the equations may appear different from those in Mike Fife's these, we assure that they are identical. Differences between the models are discussed in later sections.
In the fluid approach the behavior of the electron density, flux, and mean energy is described by the first few moments of the Boltzmann equation (transport equations); this incorporates many assumptions and is not entirely realistic. In view of the high plasma density in SPTs it is assumed that the electron density is everywhere equal to the ion density. With this assumption it becomes impossible to obtain the electric field from Poisson's equation. Instead, knowing the electron density, we use the electron transport equations to calculate the electric field.
The electron transport equations are: the continuity equation

$$\nabla\cdot\mathbf{\Gamma}_e = Nnk_i - \frac{\partial n}{\partial t} = \nabla\cdot\mathbf{\Gamma}_i\,, \tag{14}$$

the momentum equation, which we approximate by the drift-diffusion equation

$$\mathbf{\Gamma}_e = -\mu\mathbf{E}n - \frac{2}{3e}\mu\nabla(n\varepsilon), \tag{15}$$

and the energy equation

$$\frac{\partial(n\varepsilon)}{\partial t} + \frac{5}{3}\nabla\cdot(\mathbf{\Gamma}_e\varepsilon) - \frac{10}{9e}\nabla\cdot(\mu n\varepsilon\nabla\varepsilon) = -e\mathbf{E}\cdot\mathbf{\Gamma}_e - Nn\kappa - nW\,. \tag{16}$$

In these equations n is the plasma density, $\mathbf{\Gamma}_e$ the electron flux, ε the electron mean energy, N the gas density, $\mathbf{\Gamma}_i$ the ion flux, $\mathbf{E}$ the electric field, μ the electron mobility, and e the elementary charge. The last two terms in the energy equation represent energy loss by collisions with gas particles and with the walls, respectively, where κ and W are effective energy loss coefficients dependent on ε. The equations (15) and (16) assume the electron distribution to be Maxwellian and predominantly isotropic; the same assumption is used to obtain the collision coefficients k_i and κ from cross section data.
Due to the magnetic field the mobility μ is not a simple scalar: its value is much larger for electron transport along magnetic field lines than for transport across them. From current conservation however it is clear that the electron flux cannot be much larger along magnetic field lines than across them. This implies that along the field lines the two terms of equation (15) should virtually cancel each other. Taking into account similar considerations for the

electron energy flux, one can derive that the electron mean energy must be constant along magnetic field lines and that the electric potential V behaves as

$$V(x,r)=V^*(\lambda)+\frac{2}{3e}\varepsilon(\lambda)\ln\frac{n(x,r)}{n_0}, \tag{17}$$

where V^* is a function and n_0 is a reference density. While V and n vary all over space, V^* and ε depend only on the stream function λ. Note that by using this equation we lose to possibility to calculate the electron flux along magnetic field lines from the drift-diffusion equation. For the cross field electron flux on the other hand we find

$$\begin{aligned}\Gamma_{e,\perp} &= rB\mu_\perp n\frac{\partial V}{\partial\lambda}-\frac{2}{3e}rB\mu_\perp\frac{\partial(n\varepsilon)}{\partial\lambda}\\ &= rB\mu_\perp n\frac{\partial V^*}{\partial\lambda}+\frac{2}{3e}rB\mu_\perp n\left(\ln\frac{n}{n_0}-1\right)\frac{\partial\varepsilon}{\partial\lambda},\end{aligned} \tag{18}$$

where $\mu_\perp$ is now the cross field mobility, which is further discussed in Section III.A.
Let us now define the following (surface!) integrals along magnetic field lines

$$c_1=\iint\Gamma_{i,\perp}\mathrm{d}s \tag{19}$$

$$c_2=\iint rB\mu_\perp n\mathrm{d}s \tag{20}$$

$$c_3=\iint rB\mu_\perp n\left(\ln\frac{n}{n_0}-1\right)\mathrm{d}s \tag{21}$$

and (volume) integrals between consecutive field lines

$$c_4=\iiint n\mathrm{d}v \tag{22}$$

$$c_5=\iiint Nn\mathrm{d}v \tag{23}$$

$$c_6=\iiint -eE_\perp\Gamma_{e,\perp}\mathrm{d}v, \tag{24}$$

where ds and dv are surface and volume elements.
Using these integrals, the continuity and momentum equations can be replaced by the following one-dimensional equation for current conservation:

$$\iint\Gamma_{e,\perp}\mathrm{d}s=c_2\frac{\partial V^*}{\partial\lambda}+\frac{2}{3e}c_3\frac{\partial\varepsilon}{\partial\lambda}=c_1-\frac{1}{e}I, \tag{25}$$

where I is the discharge current. It is assumed that no current escapes to the walls.
In a similar way, the energy equation can be written as

$$\begin{aligned}&\frac{\partial(c_{4,k}\varepsilon_k)}{\partial t}+\frac{5}{3}\left(c_{1,k+1/2}-\frac{1}{e}\beta_{k+1/2}I\right)\varepsilon_{k+1/2}-\frac{5}{3}\left(c_{1,k-1/2}-\frac{1}{e}\beta_{k-1/2}I\right)\varepsilon_{k-1/2}\\ &-\frac{10}{9e}c_{2,k+1/2}\varepsilon_{k+1/2}\left.\frac{\partial\varepsilon}{\partial\lambda}\right|_{k+1/2}+\frac{10}{9e}c_{2,k-1/2}\varepsilon_{k-1/2}\left.\frac{\partial\varepsilon}{\partial\lambda}\right|_{k-1/2}=c_{6,k}-c_{5,k}\kappa_k-c_{4,k}W_k,\end{aligned} \tag{26}$$

where k+1/2 and k-1/2 refer to two field lines, and k to the interval between them.
From the equations (25) and (26) we calculate ε and V^* as a function of λ. Subsequently the spatial profile of the electric potential is found from equation (17). The current in the equations (25) and (26) is chosen such, that a specified voltage drop results between anode and cathode:

$$V_a-V_c=-\int_a^c\frac{\partial V^*}{\partial\lambda}\mathrm{d}\lambda+\frac{2}{3e}\varepsilon_a\ln\frac{n_a}{n_0}-\frac{2}{3e}\varepsilon_c\ln\frac{n_c}{n_0}, \tag{27}$$

where the labels a and c refer to anode and cathode, and the $n_{a,c}$ are spatially averaged over the electrode lines.

2.8 Anode region

The physics of the region in front of the anode is not well described by the above electron equations, which are solved only right of anode line, i.e. the first magnetic field line from the left that does not intercept the anode. The electron mean energy and electric potential on the

anode line and in the region left of it, where the magnetic field intercept the anode, result from boundary conditions and assumptions.
The MIT model imposes a zero energy gradient on the anode line; left of it the MIT model assumes the electrons to be fully accommodated to the anode temperature (1000 K). This leads to an unnatural discontinuity of the electron energy on the anode line; the function V^* is ajusted so as to minimize the discontinuity in the potential profile.
The CPAT model simply fixes the electron energy to a small value, typically on the order of 1 eV, not only on the anode line but also in the region left of it.
We remark that in either model too high electron mean energy at the anode (> 7 eV) leads to excessive bulk ionization there, even a global ionization maximum, which seems hardly realistic. In the MIT model this happens if the magnetic field is too strong at the anode; in the CPAT model the usual boundary condition prevents it from happening. From a physical point of view, one might imagine that collisions with anode cool the electrons.
In contrast to the CPAT model, the MIT model accounts for the voltage drop across the anode sheath when calculating the potential distribution from the electron equations. The anode sheath voltage is estimated from the classical expression

$$V_s = -\frac{kT_e}{e}\ln\left(\frac{4I}{Aenv_{th}} + \sqrt{\frac{2\pi m_e}{\hat{e}m_i}}\right) \tag{28}$$

where $kT_e = (3/2)\varepsilon$, m_e is the electron mass, m_i is the ion mass, A is the surface area of the anode, $v_{th} = (8kT_e/\pi m_e)^{1/2}$, and $\hat{e} = \exp(1)$; this is only valid for ion-attracting sheaths, i.e. V_s positive.

2.9 Downstream region

Both the MIT and CPAT models fix the electron mean energy to a few eVs on the cathode line, i.e. the magnetic field line that intercepts the anode. For the region downstream of the cathode line there is a crucial difference between the models, which we point out below.
The MIT model does not solve the electron equations in the downstream region. Instead, it defines an effective ground point, located at the utter right egde of the grid, where it sets ε and V^* to experimental values for the far-field; between the cathode and the effective ground ε and V^* are then linearly interpolated on the λ-grid. Obviously this technique does not describe the physics of the downstream region; it should be regarded as an attempt to compress the entire downstream region into the computation domain, so as to obtain a more accurate prediction for the eventual ion exhaust-velocity.
The CPAT model on the other hand solves the full set of electron equations in the downstream region. Given that for each ion leaving the thruster an electron must leave it too, the total current in the current-conservation equation (25) is set to zero here. On the right edge of the calculation domain the electron mean energy is fixed to a small value. Typically the CPAT model predicts a rise in the electric potential on the order of 10 V beyond the cathode line; further downstream the potential decreases again; this finding is supported by the experimental data in Fife's thesis [Fif98]. Accurate prediction of the final ion exhaust-velocity requires a large computation domain.

2.10 Cross field electron mobility

Cross field electron mobility is the main parameter controlling the electric potential distribution in the SPT and has therefore an enormous influence on the simulation results. [Hag01] Unfortunately it is not well known; the MIT and CPAT models use rather different assumptions for it.
The classical expression for $\mu_\perp$ is given by

$$\mu_{\perp,c} = \frac{e\nu_m/m_e}{\nu_m^2 + (eB/m_e)^2} \approx \frac{m_e \nu_m}{eB^2}, \tag{29}$$

where m_e the electron mass and ν_m the momentum-transfer frequency of electron-particle collisions. The MIT model assumes a constant momentum-transfer cross-section of 3×10^{-19} m^2 whereas the CPAT takes the momentum-transfer frequency to be constant at 2.5×10^{-13} m^3 s^{-1}; see figure 3; the CPAT model is closer to reality.

It is a known fact that the classical mobility is too small to be realistic for the electron transport in SPTs, especially near and beyond the exhaust where the gas density is very low. Both models therefore add to the classical mobility an anomalous Bohm mobility

$$\mu_{\perp,B} = \frac{K}{16B} \tag{30}$$

where K is a constant fitting parameter. Anomalous Bohm mobility has been measured in various magnetized plasma's and is usually physically interpreted as the result of plasma-field fluctuations.

The MIT model applies Bohm mobility with a factor K = 0.15 in the entire computation domain. Doing so, the model predicts the acceleration zone to be entirely located outside the channel; see CASE I in Fife's thesis [Fif98]. Since this is clearly not realistic, the MIT model moves the cathode (now called 'effective cathode') very close to the channel exhaust; this pushes the acceleration zone in; see CASE II in Fife's thesis. Note that in the MIT model the electric potential profile downstream of the cathode results from interpolation instead of from electron equations; it follows that the exterior is not really modeled at all.

The CPAT model argues that to have the acceleration zone inside the channel, the electron mobility must be much larger outside than inside. It therefore uses the Bohm mobility only outside, where K = 0.2-1; the acceleration zone is indeed found inside. It has been suggested in the litterature that the plasma flow be more stable inside due to the gradient of the magnetic field strength [Zhu99], which supports the CPAT treatment of Bohm mobility. The discontinuity in the CPAT mobility at the channel exhaust seems to have no serious consequences for the simulation results.

In addition to classical and Bohm mobility, electron-wall collisions contribute to cross-field electron transport. This is described in later sections. The various mechanisms of electron transport are compared in figure 6.

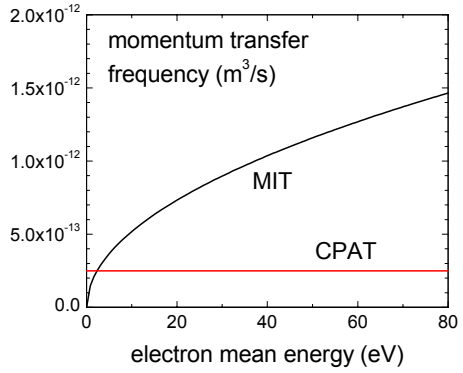

Figure 3. Comparison of ν_m/N, where N is the neutral density, assumed by the two models.

2.11 Rates of ionization and collisional energy-loss

The electron equations involve the ionization rate coefficient k_i and the collisional energy-loss coefficent κ, both as a function of electron mean energy. These coefficients result from integrating collision cross-sections over a Maxwellian electron energy distribution function. The MIT model uses theoretical data from Drawin and Dugan [Dug], the CPAT model

measured data from Puech and Mizzi [Pue91]. The resulting coefficients are somewhat different; figure 4 gives a comparison. The MIT model has a smaller ionization coefficient but a larger energy-loss coefficient. We remark that it seems odd that according to the MIT data, high energy electrons undergo an effective energy loss of about twice the ionization threshold per ionization event.

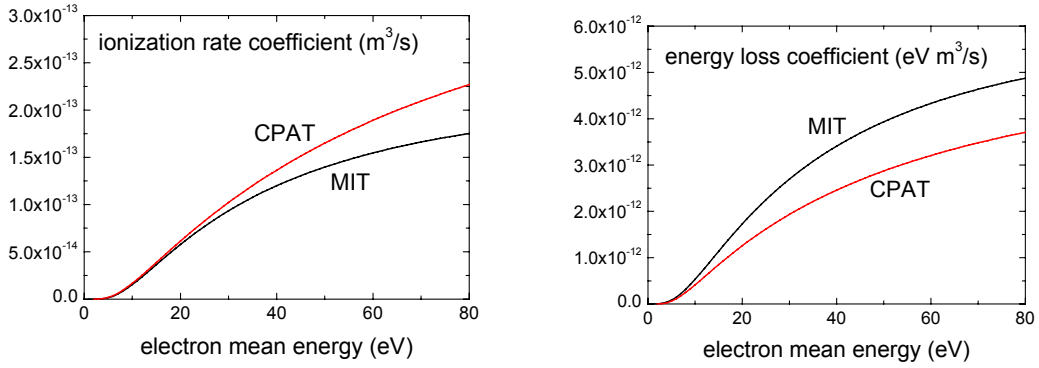

Figure 4. Comparison of the collision coefficients k_i and κ used by both models.

2.12 Wall-collision theory of the MIT model

The MIT model attempts to give a quantitative description of the effects of electron-wall collisions, taking into account electron-impact secondary emission. Here we reconstruct the MIT wall-theory from the information in Mike Fife's thesis [Fif98].
Experimental data on secondary emission are fitted as

$$\delta=\frac{\Gamma_{e,s}}{\Gamma_{e,p}}=AE^B \tag{31}$$

where $\Gamma_{e,s}$ and $\Gamma_{e,p}$ are secondary-electron and (mono-energetic) primary-electron fluxes, and E is the (mono-energetic) primary-electron impact energy. The fitting parameters A and B are typically set to 0.10-0.15 and 0.6, respectively. Note that here the secondary-electron flux represents all electrons coming off the wall, including the back-scattered primaries. By integration over a Maxwellian distribution for the primary-electron energy E the expression is found for the effective secondary-emission coefficient

$$\delta = A\,\Gamma(2+B)(kT_e/e)^B, \tag{32}$$

where Γ is Euler's gamma-function and T_e is the temperature of the primaries; in the following it is assumed that the primaries at the wall and electrons in the plasma have the same temperature T_e; this is valid for Boltzmann equilibrium in the sheath.
Subsequently the wall voltage V_w with respect to the plasma is derived from imposing zero net current to the surface. For a normal ion-attracting sheath the following balance equation is considered at the sheath edge:

$$(1-\delta)\frac{1}{4}nv_{th}\exp\left(\frac{e(V_w-V_p)}{kT_e}\right)=nv_B, \tag{33}$$

where $v_{th} = (8kT_e/\pi m_e)^{1/2}$ is the electron thermal velocity, $v_B = (kT_e/m_i)^{1/2}$ is the ion Bohm velocity, and $V_p=kT_e/e$ is the presheath voltage as predicted by the standard Bohm theory. This yields

$$V_w = -\frac{kT_e}{e}\ln\left((1-\delta)\sqrt{\frac{\hat{e}m_i}{2\pi m_e}}\right), \tag{34}$$

where $\hat{e}$=exp(1). If δ approaches 1 the sheath voltage goes positive and equation (33) is no longer valid. Instead, the wall voltage for an ion-repelling sheath found from balancing the primary- and secondary-electron fluxes, neglecting the ion flux:

$$\frac{1}{4}nv_{th}=\delta\frac{1}{4}nv_{th}\exp\left(-\frac{eV_w}{kT_{e,s}}\right), \tag{35}$$

that is

$$V_w=\frac{kT_{e,s}}{e}\ln\delta\,. \tag{36}$$

Here $T_{e,s}$ is the temperature the secondary electrons, which is typically assumed to be on the order of the wall temperature (0.1 eV). Note that the transition between the two regimes is uniquely characterized by the break-point temperature

$$T_{e,b}=\left(\frac{1-\sqrt{2\pi m_e/\hat{e}m_i}}{A\,\Gamma(B)}\right)^{1/B}, \tag{37}$$

for which δ is close to 1. Typically $T_{e,b}$ = 15 - 30 eV.

In the above sheath model the primary-electron flux to the wall is

$$\Gamma_{e,p}=\begin{cases}\frac{1}{4}nv_{th}\exp\left(\frac{eV_w}{kT_e}\right) & T_e<T_{e,b}\\ \frac{1}{4}nv_{th} & T_e>T_{e,b}\end{cases}, \tag{38}$$

where the wall voltage for $T_e<T_{e,b}$ is given by equation (34).

The MIT model goes on arguing that the secondary emission leads to a net cross-field electron transport, because the eventual orbits of the secondary-electrons are, on average, shifted towards the anode by one Larmor radius with respect to the primary-electron orbits. The resulting wall-current is shown to satisfy the equation

$$I_w=e\Gamma_{e,p}\delta\frac{2\pi r m_e E}{eB^2}, \tag{39}$$

where r is the radius of the wall. Substituting some of the above equations one finds

$$I_w=\begin{cases}n\sqrt{\frac{kT_e}{\hat{e}m_i}}\frac{\delta}{1-\delta}\frac{2\pi rEm_e}{B^2} & T_e<T_{e,b}\\ n\sqrt{\frac{kT_e}{2\pi m_e}}\,\delta\frac{2\pi rEm_e}{B^2} & T_e>T_{e,b}\end{cases} \tag{40}$$

The MIT model also predicts the electron-energy flux to the wall. For an ion-attracting sheath the primary electrons lost at the wall had, before they enterred the sheath, a mean energy equal to $2kT_e$-eV_w (V_w negative!); the emitted secondaries, once they reach the plasma, have been accerelated to a mean energy of $2kT_{e,s}$-eV_w. The net energy flux is therefore

$$q_w=(2kT_e-eV_w)\Gamma_{e,p}-(2kT_{e,S}-eV_w)\delta\Gamma_{e,p}\qquad T_e<T_{e,b}\,. \tag{41}$$

For an ion-repelling sheath on the other hand, the primary electrons are ordinary plasma-electrons with mean energy $2kT_e$ and the secondary electrons that make it to the plasma arrive there with mean energy $2kT_{e,s}$ so that the wall voltage does not interfere in the expression

$$q_w=2kT_e\Gamma_{e,p}-2kT_{e,s}\Gamma_{e,p}\qquad T_e>T_{e,b}\,.$$

Using the above equations one ends up with

$$q_w=\begin{cases}n\sqrt{\frac{kT_e}{\hat{e}m_i}}\left(\frac{2k(T_e-T_{e,s})}{(1-\delta)}+kT_e\ln\left((1-\delta)\sqrt{\frac{\hat{e}m_i}{2\pi m_e}}\right)\right) & T_e<T_{e,b}\\ n\sqrt{\frac{kT_e}{2\pi m_e}}2k(T_e-T_{e,s}) & T_e>T_{e,b}\end{cases}. \tag{42}$$

The wall current (40) and the energy loss flux (42) are explicitly taken into account in the current conservation and energy equations, respectively. For instance, the current conservation equation of the MIT model is

$$\iint\Gamma_{e,\perp}\mathrm{d}s-\frac{1}{e}(I_{w,1}+I_{w,2})=c_1-\frac{1}{e}I\,, \tag{43}$$

where $I_{w,1}$ and $I_{w,2}$ are the wall currents on the inner and outer walls.

2.13 Some remarks on the wall theory of the MIT model

1) The wall theory depends strongly on the data for the secondary-emission coefficient. What data are being used? Is the fitting formula really appropriate? The data referred to in Mike Fife's thesis, viz. measurements published by Bugeat et al. at the 1995 IEPC [Bug95], look rather limited. In the few other data that we found ourselves the mean energy of the secondary electrons (including reflected primaries) is a significant part of that of the primaries, if not close to it, i.e. much larger than $T_{e,s} \approx 0.1$ eV as assumed in the MIT model.
2) The wall theory relies heavily on the assumption of a Maxwellian electron-energy distribution. This is difficult to justify; the wall-collisions themselves can be expected to completely alter the electron energy distribution, in particular to deplete its tail. As a consequence the theory might strongly overestimate the effects of wall-collisions. In fact, deviations from Maxwellian do not only affect the wall theory but the entire electron model.
3) The wall voltage of an ion-attracting sheath includes the presheath voltage, which implies that the plasma density used to calculate the primary-electron flux to the wall (38) is to be taken outside the presheath. But where is that? Seeing that the ions are virtually collisionless, the presheath will stretch out to the center of the plasma; this wall theory is therefore not local but involves the entire plasma volume.
4) The ion model predicts the ion flux to the wall, albeit with strong statistical noise. This information could be used in the wall model to circumvent the Bohm theory and obtain more consistency. Equation (33) could then be replaced by

$$(1-\delta)\frac{1}{4} n v_{th} \exp\left(\frac{eV_w}{kT_e}\right) = \Gamma_i , \tag{44}$$

and so on. The primary-electron flux for an ion-attracting sheath would simply be

$$\Gamma_{e,p} = \frac{1}{1-\delta}\Gamma_i . \tag{45}$$

2.14 Wall effects in the CPAT model

The CPAT model does not venture into a quantitative description of electron-wall interactions and limits itself to being qualitative.
Cross-field electron transport due to wall collisions is taken into account by an additional contribution to the cross-field electron mobility. The physical interpretation of this approach is that, except for the position were they occur, there is no essential difference between electron-wall collisions and electron-particle collisions. The contribution to the mobility from the wall collisions is

$$\mu_w = \frac{m_e \nu_w}{eB^2} , \tag{46}$$

where ν_w is the momentum transfer frequency of the wall collisions, which, for the sake of simplicity, is kept constant along the channel:

$$\nu_m = \alpha 10^7 \ (\mathrm{s}^{-1}). \tag{47}$$

The fitting parameter α is typically chosen in the range 0.1-0.5.
Energy loss due to electron-wall collisions is accounted for via an empirical volumetric energy loss coefficient (energy loss per second per electron)

$$W = \alpha_\varepsilon 10^7 \varepsilon \exp\left(-\frac{U}{\varepsilon}\right) (\mathrm{s}^{-1}), \tag{48}$$

where α_ε and U are once again constant fitting parameters, typically 0.1-0.5 and 20 eV, respectively. This does not result from physical derivation, but is simply a convenient expression stating that the energy wall-loss increases monotonically, becoming important beyond the energy U.

2.15 Wall effects: local approach vs volumetric approach

The MIT model uses an explicit equation for the wall current whereas the CPAT includes it volumetrically via the electron mobility. Although at first sight these approaches may look very different, they are not.
For demonstration we translate the MIT expression for the wall current into an equivalent mobilty contribution. Consider a cross section through the channel, perpendicular to the axis. Assume that the magnetic and electric fields, the plasma density, and the electron temperature are all constant over this cross section. The wall current through the cross section in terms of a wall mobility is then

$$e\pi\left(r_2^{\,2}-r_1^{\,2}\right)\mu_w En = e\pi\left(r_2^{\,2}-r_1^{\,2}\right)\frac{m_e\nu_w}{eB^2}En\,, \tag{49}$$

where $r_{1\text{-}2}$ are the radii of the walls. Equating this to the sum of the wall currents (40) on the inner and outer walls gives

$$\nu_w = \begin{cases} \dfrac{2}{r_2-r_1}\sqrt{\dfrac{2\varepsilon}{3\hat{e}m_i}}\dfrac{\delta}{1-\delta} & \varepsilon<\dfrac{3}{2}kT_{e,b} \\ \dfrac{2}{r_2-r_1}\sqrt{\dfrac{\varepsilon}{3\pi m_e}}\delta & \varepsilon>\dfrac{3}{2}kT_{e,b} \end{cases}, \tag{50}$$

where we substituted $kT_e = (3/2)\varepsilon$.
Similarly, the MIT energy flux to the wall can be written in the form of the volumetric energy loss coefficient W. Integrating the energy loss over a slice perpendicular to the axis and with a thickness d one obtains the equation

$$\pi\left(r_2^{\,2}-r_1^{\,2}\right)d\; nW \;=\; 2\pi\left(r_1+r_2\right)d\; q_w\,, \tag{51}$$

which yields

$$W = \begin{cases} \dfrac{2}{r_2-r_1}\sqrt{\dfrac{2\varepsilon}{3\hat{e}m_i}}\left(\dfrac{4\varepsilon-4\varepsilon_s}{3(1-\delta)}+\dfrac{2}{3}\varepsilon\ln\left((1-\delta)\sqrt{\dfrac{\hat{e}m_i}{2\pi m_e}}\right)\right) & \varepsilon<\dfrac{3}{2}kT_{e,b} \\ \dfrac{2}{r_2-r_1}\sqrt{\dfrac{\varepsilon}{3\pi m_e}}\delta\dfrac{4}{3}\left(\varepsilon-\varepsilon_s\right) & \varepsilon>\dfrac{3}{2}kT_{e,b} \end{cases}. \tag{52}$$

Note however that there are some minor differences between the explicit approach of the MIT model and the equivalent volumetric approach:

1) In the MIT model the wall effects are calculated from the local fields and plasma density at the walls, whereas the volumetric treatment averages over the volume. It is not clear that locality is an advantage here, given the fact that the presheath extends far into the plasma; see also remark 3) of section 2.13.
2) The MIT wall-current (40) is directly proportional to the electric field, whereas with the volumetric treatment wall collisions also lead to a diffusion flux. The latter does not seem less realistic than the first.

2.16 Wall effects: MIT model vs CPAT model

Using the volumetric equivalents presented in the previous section, one can directly compare the MIT wall-theory with the empirical CPAT formulas. This is done in figure 5 for typical values of the various fitting parameters.
In order to give an idea of how the wall-effect relate to the rest of the model, figure 6 compares them with competing volume effects, discussed in previous sections; each of the plots in this figure is based on the same data for the magnetic field, neutral density, and electron mean energy, obtained with a standard simulation that is further described in the chapter on code-to-code validation.

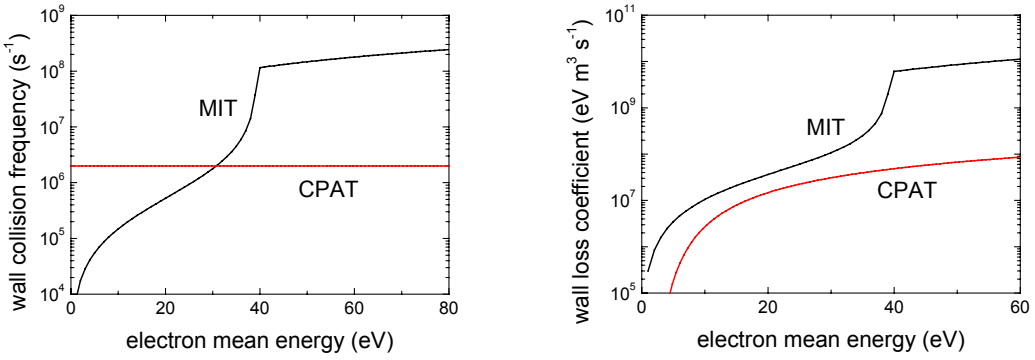

Figure 5. Comparison between the wall-collision frequencies and energy-loss coefficients of the MIT and CPAT models. On the left the functions (47) and (50) are plotted, on the right the functions (48) and (52). The fitting parameters are set to standard values: $A = 0.108$, $B = 0.576$, $\varepsilon_s = 0.1$ eV for the MIT model and $\alpha = \alpha_\varepsilon = 0.2$, $U = 20$ eV for the CPAT model.

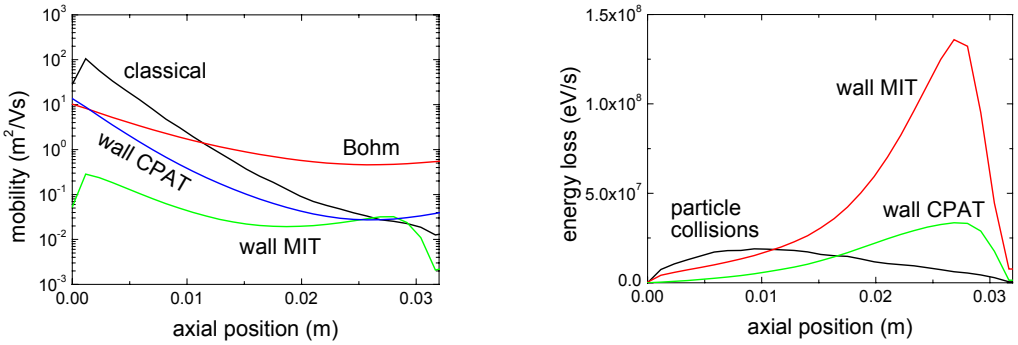

Figure 6. Comparison of the wall effects in the MIT and CPAT models with competing volume effects. The plots show axial profiles in the center of the channel for a typical simulation, which is described in more detail in chapter 3. The anode cathode are located on the left and on the right, respectively. The Bohm parameter $K = 0.15$, the wall fitting parameters are set to the same standard values as with the previous figure.

2.17 Numerical solution of the electron equations

The solution of the electron equations is tough numerical task that is handled very differently by the two models.

The MIT model solves the electron energy equation by a modified Forward Time Centered Space method: the energy is updated fully explicitly and all differentials are approximated by central differences on the λ-grid. This technique necessitates the use of a very small time step, typically 5×10^{-11} s, so that many iterations must be performed to simulate a significant period of SPT operation. We remark that central differences are not appropriate for the first-order terms in space if they dominate the second-order terms; in practice however this must not be the case since the MIT method turns out to work reasonably well.

The CPAT model evaluates the spatial differences fully implicitly, using a very robust exponential discretization scheme [Sch69]. The energy loss terms are evaluated implicitly by a Newton iteration, i.e. the terms are linearized in energy around the value of the previous iteration. [Hag00] The implicit technique avoids strong time step restictions; time steps of 10^{-8} s or more can be used without problem. As a result, the computation time spent on solving the electron equation is negligible in the CPAT model.

3 CODE-TO-CODE VALIDATION

In order to check for gross numerical errors in the models and thus give more confidence in their results, we have directly compared them on the simulation of the SPT-70. For this purpose the models were slightly modified so as to represent as much as possible the same physical equations. The modifications included the following:

1) Double ionization was turned off in the MIT model.
2) The MIT wall-theory was included in the CPAT model via the equivalent wall-mobility and energy wall-loss coefficient.
3) The MIT data for the ionization coefficient, the energy-loss coefficient, and classical electron mobility, were implented into the CPAT model.
4) Bohm mobility inside the channel was added to the CPAT model.
5) The cathode in the CPAT model was placed close to the exhaust, as in the MIT model.
6) The potential drop across the anode sheath as calculated by the MIT model was explicitly added to the applied voltage in the CPAT model.

In spite of these changes some differences were still present:

1) Since the CPAT treatment of the region downstream of the cathode is on no account compatible with the MIT assumptions on the electron mobility, it was decided to completely turn off the CPAT simulation of this region; the MIT model still used its usual interpolation technique. Note that the downstream region is not expected to have much influence on the discharge inside the channel.
2) The boundary conditions on the anode were left as is: In the region left of the anode line the MIT model assumes the electron mean energy to be 0.1 eV, whereas the CPAT model uses the same value as on the anode line, about 6 eV in this case.
3) The volumetric CPAT treatment of wall-effects is slightly different from the local MIT treatment; see section 2.15.

Standard input data and conditions were used: magnetic field as in Fife's thesis, applied voltage 300 V, debit 2.34 mg/s, Bohm parameter $K = 0.15$, wall parameters $A = 0.108$, $B = 0.576$, $\varepsilon_s = 0.1$ eV.
The two codes turned out to yield very similar simulation results indeed, in spite of their very different numerical methods; see figures 7 and 8. Not only the time-averaged spatial results are close together, but also the temperoral behavior and calculated oscillations. The minor differences in the results can easily be attributed to the above-mentionned differences that remained in the physical equations, and do not give rise to doubts about the numerical implementation of the models.

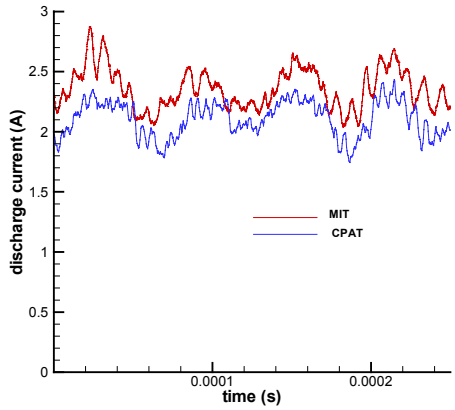

Figure 7. Comparison of the discharge currents calculated by the MIT and CPAT models, modified to represent similar physics, for a standard simulation of the SPT-70.

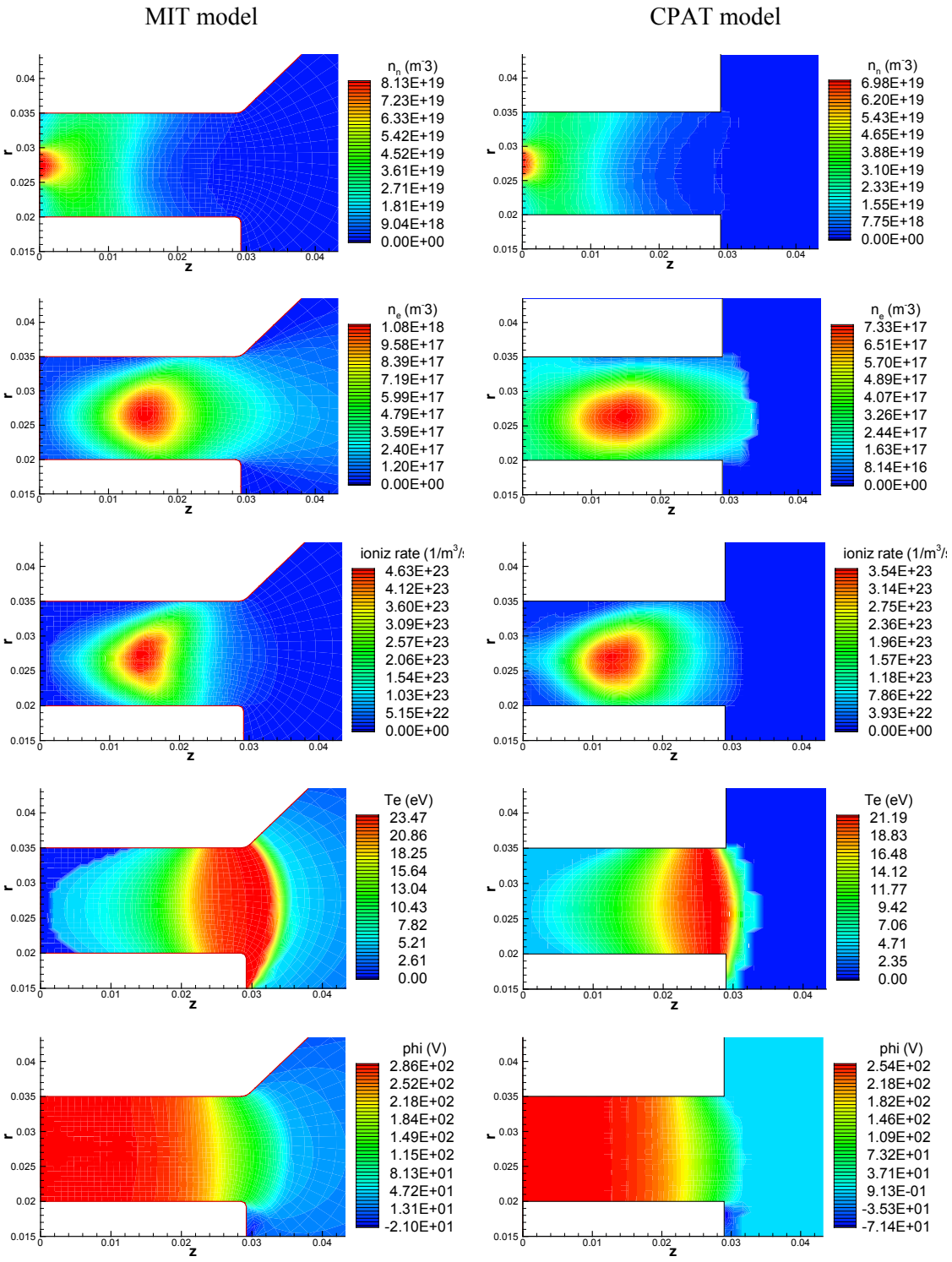

Figure 8. Direct comparison of the MIT and CPAT models, modified to represent similar physics, on a standard simulation of the SPT-70. The plots show time-averaged two-dimensional profiles of the neutral density, plasma density, ionization rate, electron mean energy, and electric potential, respectively; on the left-hand side the MIT model, right the CPAT model.

4 CONCLUSIONS

There are two major differences in the physics of the MIT and CPAT models:

1) The MIT model estimates the effects of electron-wall collisions from a sheath theory, taking into account electron-impact secondary-electron emission, whereas the CPAT model uses simple empirical formulas. Although the MIT model approach seems more advanced, it is based on many questionnable assumptions.
2) The MIT model uses the same Bohm conductivity everywhere, while CPAT model uses Bohm conductivity only outside. With the MIT approach the cathode must be placed near the exhaust to obtain an acceleration zone inside the channel; the region beyond the cathode cannot be simulated and is described by interpolation to a ground point. The CPAT approach automatically locates the acceleration zone inside the channel and allows the full simulation of the downstream region.

These differences mark the points were the physics is the least understood and the assumptions are the most doubtful. Without new experimental evidence, significant improvement of the models seems unlikely.

When modified to represent similar physics, the models yield very similar results. Not only the time-averaged spatial results are close together, but also the temperoral behavior and calculated oscillations. This is strong evidence that there are no gross numerical errors in either of the codes.

References

[Bir94] G. A. Bird, Molecular gas dynamics and the direct simulation of gas flows, (Clarendon Press, Oxford, 1994).

[Bug95] J. P. Bugeat and C. Koppel, 24th International Electronic Propulsion Conference, paper IEPC-95-240 (Moscow, Russia, 12-23 September 1995)

[Dug] J. V. Dugan and R. J. Sovie, NASA report TN D-4150.

[Fif98] J. M. Fife, Ph.D. thesis (Massachusettes Institute of Technology, 1998).

[Hag00] G. J. M. Hagelaar and G. M. W. Kroesen, J. Comp. Phys. **159**, 1 (2000).

[Hag01] G. J. M. Hagelaar *et al.*, 27th International Electronic Propulsion Conference, paper IEPC-01-28 (Pasadena, California, USA, 15-19 October 2001)

[Hag02] G. J. M. Hagelaar, J. Bareilles, L. Garrigues, end J.-P. Bœuf, accepted for publication in J. Appl. Phys.

[Pue91] V. Puech and S. Mizzi, J. Phys. D **24**, 1974 (1991).

[Sch69] D. L. Scharfetter and H. K. Gummel, IEEE Trans. Electron Devices ED **16**, 64 (1969).

[Zhu91] V. V. Zhurin, H. R. Kaufmann, and R. S. Robinson, Plasma Sources Sci. Techn. **8**, R1 (1999).